

Role of Oxidized Gly25, Gly29, and Gly33 Residues on the Interactions of A β _{1–42} with Lipid Membranes

Hebah Fatafta, Chetan Poojari, Abdallah Sayyed-Ahmad, Birgit Strodel, and Michael C. Owen*

Cite This: *ACS Chem. Neurosci.* 2020, 11, 535–548

Read Online

ACCESS |

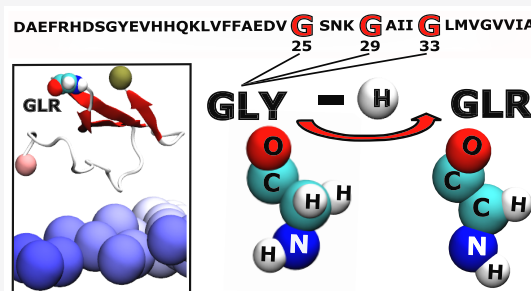
Metrics & More

Article Recommendations

Supporting Information

ABSTRACT: Oxidative stress is known to play an important role in the pathogenesis of Alzheimer's disease. Moreover, it is becoming increasingly evident that the plasma membrane of neurons plays a role in modulating the aggregation and toxicity of Alzheimer's amyloid- β peptide ($A\beta$). In this study, the combined and interdependent effects of oxidation and membrane interactions on the 42 residues long $A\beta$ isoform are investigated using molecular simulations. Hamiltonian replica exchange molecular dynamics simulations are utilized to elucidate the impact of selected oxidized glycine residues of $A\beta$ 42 on the interactions of the peptide with a model membrane comprised of 70% POPC, 25% cholesterol, and 5% of the ganglioside GM1. The main findings are that, independent of the oxidation state, $A\beta$ prefers binding to GM1 over POPC, which is further enhanced by the oxidation of Gly29 and Gly33 and reduced the formation of β -sheet. Our results suggest that the differences observed in $A\beta$ 42 conformations and its interaction with a lipid bilayer upon oxidation originate from the position of the oxidized Gly residue with respect to the hydrophobic sequence of $A\beta$ 42 involving the Gly29-XXX-Gly33-XXX-Gly37 motif and from specific interactions between the peptide and the terminal sugar groups of GM1.

KEYWORDS: Amyloid- β peptide, molecular dynamics, membrane simulations, oxidative stress, GM1, peptide membrane interactions



1. INTRODUCTION

Alzheimer's disease (AD) is a neurodegenerative disorder generally affecting persons 65 years and older.¹ With no cure currently available, and the generally increasing life expectancy in most societies, the number of people affected by this disorder is expected to increase in the coming years. Several mechanisms have been proposed as the pathological cause of AD, including genetics, cholinergic, tau, and amyloid hypotheses.^{2–6} Though no hypothesis has been generally accepted, AD brain features substantiate the most widely accepted amyloid cascade hypothesis.⁷ In particular, the AD brain is characterized by the presence of senile plaques. The main component of these plaques is the amyloid- β peptide, which is produced by the cleavage of the amyloid precursor protein (APP) by β and γ secretases.^{8–10} $A\beta$ ranges from 39 to 43 amino acids in length; however, $A\beta$ 42 is predominant in senile plaques and is known to be more toxic than $A\beta$ 40.^{11–13} The primary structure of $A\beta$ 42 is shown in Figure 1. It extends from the unstructured hydrophilic N-terminal region (Asp1 to Lys16) to the hydrophobic C-terminal region (Ala30 to Ala42), and it is linked by central residues (Leu17 to Gly29) that most often form a turn conformation. The central residues have been shown to play a role in membrane insertion and side chain–side chain interactions through a backbone bend that brings the two β -sheets together.^{14–18} In addition, the AD brain is commonly characterized by an increase in oxidative stress.^{19–23} The generation of excess reactive oxygen species

(ROS) or the dysfunction of the antioxidant system can cause an increase in the amount of ROS present in normal cells and subsequently leads to the oxidative stress observed in AD.^{24,25} The ROS are produced either enzymatically (for example to kill invaders in macrophages) or as a side reaction (like respiratory chain) and generally kept at low level but not totally eliminated due to their function. They are necessary to maintain homeostasis in cells and play an important role in signaling. The brain seems to be sensitive to oxidative damage upon oxidative stress due to high dioxygen (the final electron acceptor) consumption in the brain, approximately 20% of the total body consumption.²⁶ It is still controversial whether the accumulation of $A\beta$ increases the level of oxidative stress or that the high level of oxidative stress drives $A\beta$ accumulation.⁶ Studies have shown that $A\beta$ is capable of generating free radicals^{27,28} and shows high affinity to bind metals such as Cu^{2+} and Zn^{2+} .^{29–31}

Though the physiological role of $A\beta$ is not well understood, it was found that $A\beta$ -membrane interactions are essential for $A\beta$ to fulfill its physiological functions. These functions include protecting the body from infections, repairing leaks in the

Received: October 16, 2019

Accepted: January 15, 2020

Published: January 15, 2020

studies have been attempted to explore the effect of radicals on proteins, but challenges in locating the center of a radical in protein hinders systematic experimental investigations.^{57,58}

Studies of $A\beta$ peptide often employ shorter $A\beta$ analogs; however, it is essential to explore the full-length monomeric form of $A\beta$ for a comprehensive understanding of its toxicity.^{59,60} Unfortunately, exploring the full-length of $A\beta$ is experimentally challenging due to its high propensity to aggregate. Alternatively, MD simulations can provide insight into the conformational dynamics of $A\beta$ at atomistic resolution and complement experimental findings.^{61,62} Previously, MD simulations have been used to investigate the effect of protein oxidation on protein folding. Owen and co-workers examined the effect of C_{α} -centered radical formation on the stability of a model helical peptides in different solvent systems.⁶³ Moreover, MD simulations demonstrated the effect of glycine residue radicalization on protein conformation depends both on the protein and the position of the radical.⁶⁴ The effect of radicalization at Gly25 on the $A\beta$ 42 dimer in solution was further investigated by Liao et al.⁶⁵ Although the occurrence of oxidative stress in several neurodegenerative diseases is well-established, there is no computational evidence on the effect of radicalization on peptide-membrane interactions.

Thus, in this study we employ Hamiltonian replica exchange molecular dynamic (HREMD) simulations to understand the effect of oxidizing glycine residues (25, 29, and 33) on the $A\beta$ 42 secondary structure and membrane binding. The structures of 1-palmitoyl-2-oleoyl-phosphatidylcholine (POPC), monosialotetrahexosylganglioside (GM1), and cholesterol (CHOL) used in this membrane are shown in Figure 2. The parameters of the glycy radical (GLR) are taken from our previous study,⁶⁶ and the structure of GLR is shown in Figure S1 in the Supporting Information. HREMD simulations provide an advantage over MD in that it enhances the conformational sampling of the phase space and overcomes the problem of restricting the system to localized low energy regions of the conformational space.⁶⁷

2. RESULTS AND DISCUSSION

Understanding the neuropathology of Alzheimer's disease (AD) is the driving engine for most research in chemical neuroscience and biology. It is thought that the development of Alzheimer's disease (AD) is related to the interactions between amyloid- β ($A\beta$) with neuronal membranes. However, it has also found that the AD brain is characterized by an increase in oxidative stress. This research aims at a better understanding of this complex relationship by examining the effect of oxidizing selected glycine residues in $A\beta$ 42 on its potential toxicity and interaction with a lipid membrane containing the GM1 ganglioside. That would help toward better understanding of this neurodegenerative disorder and its treatment.

2.1. Effect of Bilayer on $A\beta$ 42. **2.1.1. $A\beta$ 42 Insertion Distance.** To see which peptide residues most frequently interacted with the bilayer, we calculated the average distance between the COM of each residues and the average position of each lipid type along the bilayer normal (z -axis). The time-averaged z -position of the phosphorus atom of POPC was used as a reference by setting their average position to zero. The relative position of the hydroxyl oxygen of cholesterol and the COM of the GM1 headgroup are shown in Figure 3. On average, the center of mass of the GM1 headgroups is above

the phosphate group of POPC, while the hydroxy group of cholesterol lies beneath it.

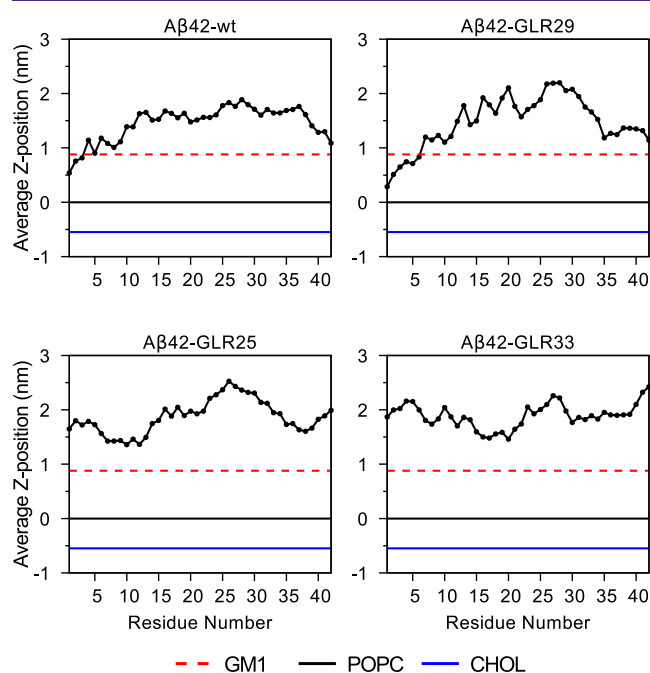


Figure 3. Average insertion distance of each $A\beta$ 42 residue with respect to the POPC and GM1 headgroups and the CHOL hydroxyl group. The headgroups of GM1, POPC, and CHOL are shown in red, black, and blue, respectively.

It can be seen in Figure 3 and Figure 4 that $A\beta$ 42-wt and $A\beta$ 42-GLR29 show similar bilayer interaction profiles, whereas both $A\beta$ 42-GLR25 and $A\beta$ 42-GLR33 had similar interaction profiles. In the wild-type $A\beta$ 42 and $A\beta$ 42-GLR29, Asp1 is closest to the phosphate atoms of the POPC lipids. Its distance from POPC is around 0.5 nm in the former and 0.3 nm in the latter peptide. N-terminal residues Ala2 to Arg5 are the next closest to the bilayer in both cases. The residues in the central polar region (Ser26 to Lys28) were the furthest from the bilayer, whereas residues Ala30, Ile32, Val36, and Gly37 from the C-terminal hydrophobic region of the wt and residues Lys16 and Phe20 of $A\beta$ 42-GLR29 were the next furthest. Despite these similarities, $A\beta$ 42-GLR29 stays slightly closer to the bilayer than the wild-type $A\beta$ 42 does. In the case of $A\beta$ 42-GLR25 and $A\beta$ 42-GLR33, the former is on average the furthest from the bilayer, and this is more pronounced in the N- and C-terminal regions. In the case of $A\beta$ 42-GLR25, the central polar region residues Glu22 to Gly29 are the furthest from the bilayer.

To analyze whether the binding of $A\beta$ 42 to the membrane has an effect on the membrane properties, we first calculated the average bilayer thickness based on the positions of the phosphorus atoms for each simulated system. The average bilayer thickness was found to be about 4.5 nm for all studied systems (see Table S1). This average value was then compared to the local bilayer thickness that was calculated for the snapshots of each trajectory where $A\beta$ 42 was bound to the membrane. To this aim, we utilized the GridMAT-MD tool^{68,69} to calculate the local membrane thickness averaged over all HREMD snapshots containing at least one atom of $A\beta$ 42 within 0.5 nm of the lipid bilayer. The resulting 2D plots (Figure S2) reveal a reduction in the local bilayer thickness to

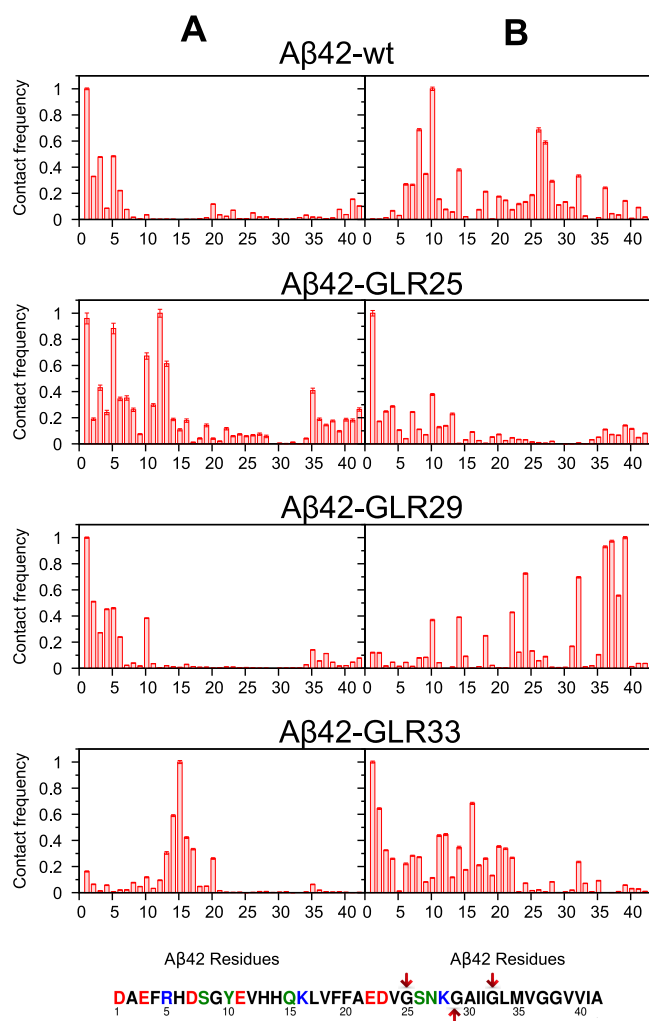


Figure 4. Contact frequency of each $A\beta 42$ residue (and standard deviation of the mean) with POPC (A) and GM1 (B) headgroups. The figure shows the normalized contact frequency in the range 0 to 1, such that 1 means the residue always made contacts with the lipid, and zero means no contacts were made. The sequence of the $A\beta 42$ residues is shown below.

about 4.4 nm or even less upon the interaction of the peptide with the lipid headgroups.

2.1.2. $A\beta 42$ Contacts and Hydrogen Bond with the Bilayer. For a greater understanding of which $A\beta 42$ residues associated with the bilayer, the number of contacts between each $A\beta 42$ residue and the bilayer for the 4 systems was calculated and normalized in the range of 0 to 1, where 0 means that the residue made no contact with the lipid in question, and 1 stands for residues that always remained in contact with lipid (see Figure 4).

The N-terminal residues of $A\beta 42$ -wt made the most contacts with POPC lipids. In this region Asp1 formed the most contacts, followed by Arg5, Glu3, and Ala2, respectively, and then His6, Asp7, and Tyr10 from the metal binding region. Fewer contacts, with a normalized contact frequency of less than 0.2, were observed in the central polar and the C-terminal hydrophobic regions. Similarly, the contacts between $A\beta 42$ -GLR29 residues and POPC were dominated by the N-terminal residues, with a higher membrane affinity shown here in this peptide residues than those in the wild-type. In this region the most contacts were made by Asp1, and the next highest is Ala2,

followed by Arg5, Phe4, and Glu3, respectively, and then Tyr10 in the metal binding region. Fewer contacts (a normalized frequency of less than 0.2) were observed in the C-terminal region, and almost no contacts were made between the bilayer and the central polar and central hydrophobic regions of the peptide. On the other hand, the contacts between $A\beta 42$ -GLR25 and POPC were dominated by residues from the metal binding region. In this region, contacts with residues Asp1, Arg5, Tyr10, Val12, and His13 were most frequent. Fewer contacts, with a normalized frequency of less than 0.5, were observed among the remaining residues in this region and the C-terminal hydrophobic regions. $A\beta 42$ -GLR33 has the lowest affinity for POPC. The most contacts in this peptide were made by residues 13 to 17 from the metal-binding region, with a normalized frequency greater than 0.3.

Most $A\beta 42$ residues showed a propensity to bind GM1 in both the wt and oxidized peptides. However, the contact frequency in the metal-binding region is the highest in $A\beta 42$ -GLR33, followed by $A\beta 42$ -wt, $A\beta 42$ -GLR25, and $A\beta 42$ -GLR29. The central hydrophobic core and the central polar region had the highest affinity for GM1 in $A\beta 42$ -GLR33, followed by $A\beta 42$ -wt, $A\beta 42$ -GLR29, and $A\beta 42$ -GLR25, respectively. These contacts are almost abolished in the case of POPC. The C-terminal hydrophobic region showed the highest frequency to bind GM1 in $A\beta 42$ -GLR29 followed by $A\beta 42$ -wt, $A\beta 42$ -GLR33, and $A\beta 42$ -GLR25, respectively.

Residues Asp1 and Arg5 in the metal-binding region of $A\beta 42$ -wt and both $A\beta 42$ -GLR25 and GLR29 formed hydrogen bonds with POPC, as shown in Figure 5. The propensity to form hydrogen bonds between $A\beta 42$ and POPC is higher in the metal-binding region of $A\beta 42$ -wt and $A\beta 42$ -GLR29 than in $A\beta 42$ -GLR25, while it is less than 10% in some residues within the metal-binding region of $A\beta 42$ -GLR33. On the other hand, no hydrogen bonds formed between POPC and the central polar and C-terminal regions of any of the four $A\beta 42$ peptides.

The propensity of hydrogen bonds to form with GM1 is higher in the case of the oxidized $A\beta 42$ -GLR25, $A\beta 42$ -GLR29, and $A\beta 42$ -GLR33 than in the wt $A\beta 42$. The C-terminal hydrophobic residues of $A\beta 42$ tended to form hydrogen bonds with GM1, which was not the case with POPC. The highest hydrogen bond propensity of the C-terminal hydrophobic residues was observed in $A\beta 42$ -GLR29.

2.1.3. $A\beta 42$ Bilayer Interaction Energy. Next, we analyzed whether the contacts between $A\beta 42$ residues and the lipid bilayer were driven by electrostatic or Lennard-Jones (LJ) interactions. The strongest Coulombic interactions (Figure S3) between POPC and $A\beta 42$ -wt were at Asp1 at $-256 \text{ kJ}\cdot\text{mol}^{-1}$, and the next strongest interacting residue was Arg5; however, the interaction strength at Arg5 was only 1/5 of that at Asp1. The Coulombic interactions between $A\beta 42$ -GLR29 and POPC showed a similar trend as the wt, but the interaction energy of Asp1 was weaker, at around $-150 \text{ kJ}\cdot\text{mol}^{-1}$ and around $-20 \text{ kJ}\cdot\text{mol}^{-1}$ at Tyr10 compared to zero in the wt. The Coulombic interactions between POPC and $A\beta 42$ -GLR25 and $A\beta 42$ -GLR33 are less than $-20 \text{ kJ}\cdot\text{mol}^{-1}$ with residues Asp1 in the former peptide and His13 to Lys16 in the latter peptide. The Coulombic interactions with GM1 were stronger in $A\beta 42$ -GLR25 and $A\beta 42$ -GLR33 compared to $A\beta 42$ -wt and $A\beta 42$ -GLR29. The strongest interaction was with Asp1 in $A\beta 42$ -GLR25 and with Lys16 in $A\beta 42$ -GLR33 with interaction strengths of -104 and $-60 \text{ kJ}\cdot\text{mol}^{-1}$, respectively. The next strongest interaction between GM1 and $A\beta 42$ -GLR33 was with Asp1 at $-50 \text{ kJ}\cdot\text{mol}^{-1}$. Overall, the attractive Coulombic

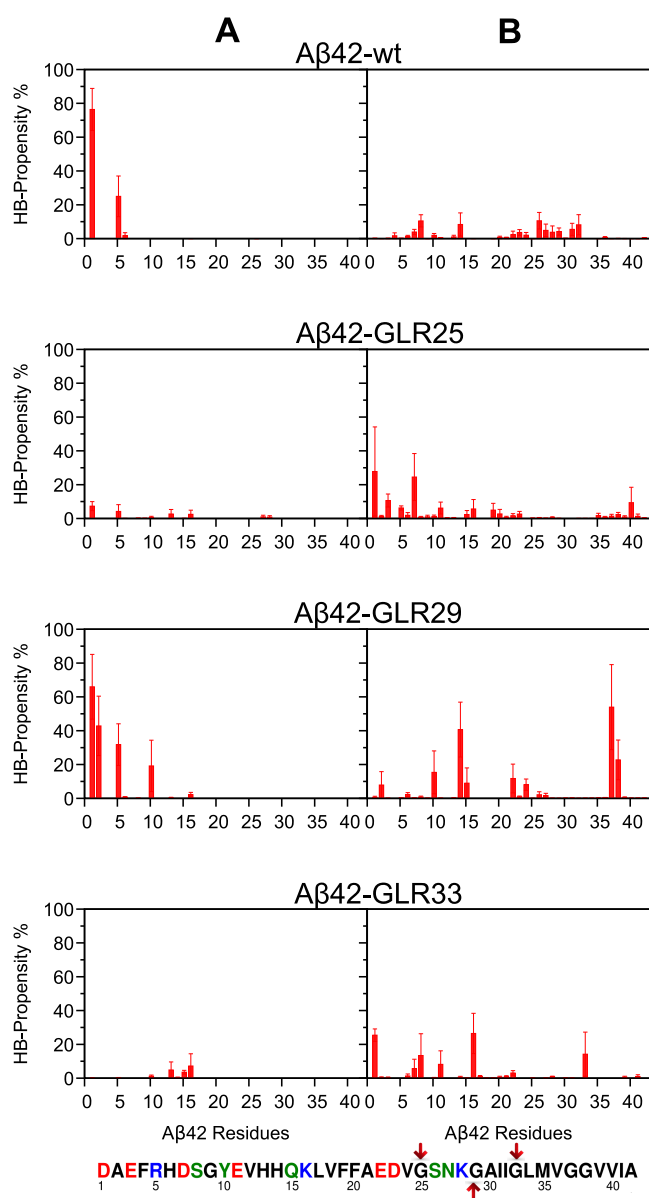


Figure 5. Hydrogen bond propensity (and standard deviation of the mean) of each $A\beta 42$ residue with (A) POPC and (B) GM1 headgroups.

interactions with GM1 were lower in magnitude compared to those with POPC, where no single residue had an average interaction energy below $-104 \text{ kJ}\cdot\text{mol}^{-1}$.

The profile of the LJ interaction energies (Figure 6) between each $A\beta 42$ peptide and the lipids was very similar to that of their respective contact frequency figure (Figure 4). For $A\beta 42$ -wt and $A\beta 42$ -GLR29 the strongest LJ interactions with POPC were in the N-terminal region of the peptides and averaged between -10 and $-13 \text{ kJ}\cdot\text{mol}^{-1}$. In $A\beta 42$ -GLR33 the strongest LJ interactions were with residues His13 to Gln15, whereas residues in the central hydrophobic region averaged between -0.7 and $-11 \text{ kJ}\cdot\text{mol}^{-1}$. Similarly, the strongest LJ interaction with GM1 was on average $-10 \text{ kJ}\cdot\text{mol}^{-1}$ in the C-terminal region of $A\beta 42$ -GLR29 and both the metal binding and the central hydrophobic regions of $A\beta 42$ -GLR33. The LJ interactions of $A\beta 42$ -GLR25 with GM1 averaged less than $-10 \text{ kJ}\cdot\text{mol}^{-1}$ and was dominated by residues from the metal

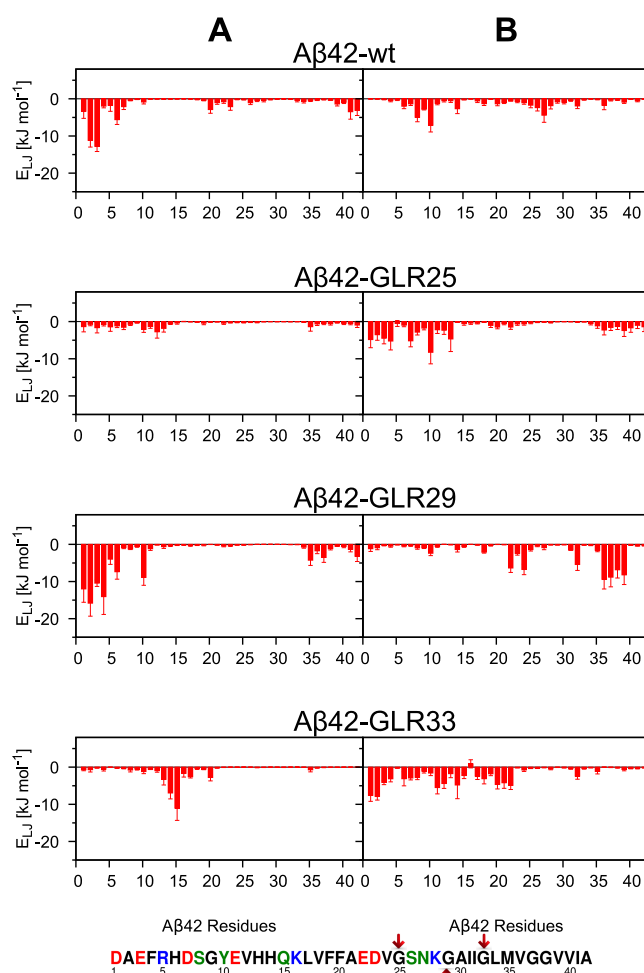


Figure 6. Lennard-Jones interaction energy of each $A\beta 42$ residue (and standard deviation of the mean) between $A\beta 42$ and POPC (A) and GM1 (B) headgroups.

binding and the C-terminal hydrophobic regions. It averaged less than $-5 \text{ kJ}\cdot\text{mol}^{-1}$ in the case of the wt $A\beta 42$.

Furthermore, we examined the effect of solvation on peptide–lipid interactions, to ensure that the stronger the peptide–lipid interaction the lesser the peptide is susceptible to solvation effects. To this aim, the time evolution of the number of water molecules within a 0.5 nm shell from the C atom of the peptide^{70,71} and the minimum distance of the peptide C_α atoms from the lipids were calculated and are jointly shown in Figure S4. A decreasing peptide distance from the lipid (i.e., stronger peptide–lipid interactions) correlates with a reduction in the peptide hydration. Moreover, the highest population of solvating water molecules was present at approximately 3 nm distance of $A\beta$ from the membrane surface, i.e., the initial distance, and it takes around 50 ns for the peptide to move closer to the lipids.

2.2. $A\beta 42$ Structural Properties. **2.2.1. $A\beta 42$ Secondary Structure Assignment.** In the wild-type $A\beta$, residues Phe4 to Glu11 displayed a β -turn/bend structure. Residues Val12 to Gln15 displayed a helical structure. Residues Lys16 to Ala21 showed a mixture of helical and β -turn/bend structures. Residues Glu22 to Val39 showed a β -turn/bend structure with residues Ile32, Leu34, Val36, and Val39 displaying a mixture of a β -strand/bridge and helical structure. Residues Met35, Val40, and Ile41 showed a β -strand/bridge.

Similar to what was seen in the wild-type, all oxidized A β peptides showed a high propensity to form a helical structure in the region Glu11 to Ala21 (Figure 7), with the lowest

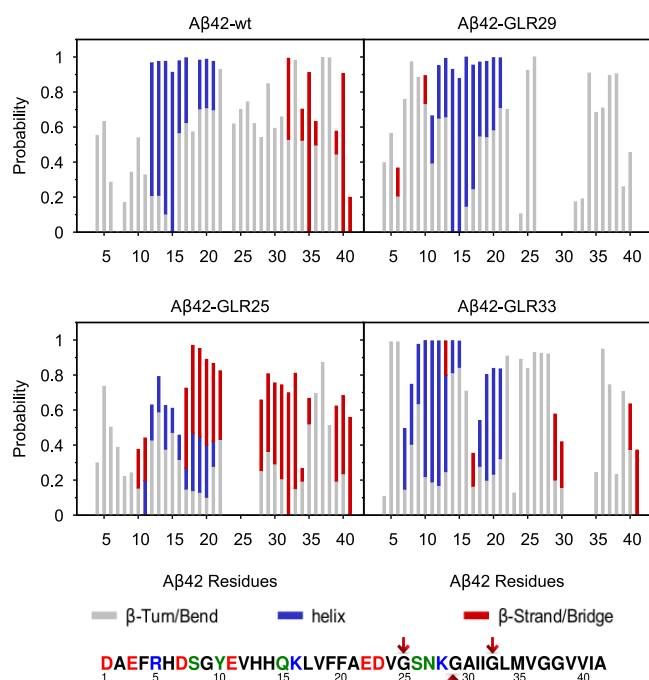


Figure 7. Secondary structure assignment of each A β 42 residue in the case of A β 42-wt, A β 42-GLR25, A β 42-GLR29, and A β 42-GLR33 in a bilayer compromised of 70% POPC, 25% CHOL, and 5% GM1. The β -turn/bend is shown in silver, the helix is shown in blue, and the β -strand/bridge is shown in red. The figure shows the additive probability of all secondary structures such that the maximum is 1; those residues showing a probability lower than 1 form random coil.

propensity observed in the case of A β 42-GLR25. However, an increase in helicity was observed in the case of A β 42-GLR33, such that the helical region extended to include residues Asp7 to Ala21 from the central polar and central hydrophobic regions.

The propensity to form a β -strand/bridge was the highest in A β 42-GLR25 and A β 42-wt. Few residues in A β 42-GLR29 and A β 42-GLR33 showed a β -strand/bridge structure. This includes residues His6 and Tyr10 in the former peptide and residues His13, Leu17, Gly29, Ala30, Val40, and Ile41 in the latter peptide. On the other hand, all A β 42 peptides showed a higher probability to form a β -turn/bend. Interestingly, residues Asp23 to Asn27 in A β 42-GLR25, residues Asn27 to Ile31 in A β 42-GLR29, and residues Ile31 to Leu34 in A β 42-GLR33 did not show any turn/bend structure.

Moreover, the development of the secondary structure content for all simulations as a function of the simulation time was analyzed and shown in Figure S5. To this aim we utilized the moving window statistics (more about the method can be found in the figure caption) to test the convergence of the secondary structure during the simulation.^{71,72} The figure shows good agreement in the overall trend of the β -sheet propensity over different time windows, and the secondary structure propensity of the peptides apart from A β 42-GLR25 converges after 80 ns as no further changes in the β -sheet propensity are observed by the end of the simulations. A β 42-GLR25 is more flexible than the other three peptides and thus needs more time for the secondary structure to converge. This

is in line with the previous findings by Liao et al., who found that the flexibility of A β 42 increases upon oxidation of Gly25.⁶⁵ Nonetheless, within the last 40 ns of the HREMD simulation also this simulation converged as supported by the nearly stable β -sheet propensity for each of the residues.

2.2.2. A β 42 Intramolecular Hydrogen Bond and Contact. Hydrogen bonds present within the peptide backbone, the peptide side chains, and between the peptide backbone and side chains that were present for more than 40% of the time were recorded and listed in Table S2. In the wild-type A β 42, backbone–backbone hydrogen bonds were present in the C-terminal region between Ile41 with Gly33 and Leu34, Ile31 with Leu34 and Met35, Gly33 and Met35, and Val36 and Val39, which stabilizes the β -sheet structure. They are also present between residues from the metal binding region such as Glu11 with His14 and Gln15, Val12 and Lys16, His14 with Leu17 and Val18, and Val18 with Ala21 from the central hydrophobic region. In the N-terminal region, backbone-side chain hydrogen bonds formed between Glu3 with Phe4 and Arg5. Moreover, hydrogen bonds formed between the side chain of Glu3 (hydrogen bond acceptor) and the side chain of Arg5 (hydrogen bond donor) from this region. Similarly, a lower number of backbone–backbone hydrogen bonds were present in the A β 42-GLR33 metal binding and C-terminal regions. On the other hand, A β 42-GLR29 and A β 42-GLR25 contained additional backbone–backbone hydrogen bonds that formed within the central hydrophobic core, within the central polar region, and between the C-terminal and the central polar region in the former and within the polar region and between the C-terminal and the central hydrophobic cores of the latter. These bonds exist between residues that either form helices or β -sheets, and such structures are discussed in the next section about the most prevalent A β 42 structures. Residues in the N-terminal region did not form backbone to backbone hydrogen bonds in any of these peptides.

The backbone–side chain hydrogen bonds formed most often in A β 42-GLR33. However, Phe4 formed a hydrogen bond with Glu3 and Arg5 in all peptides except A β 42-GLR25, which did not form any backbone–side chain hydrogen bonds. The hydrogen bonds involving side chains in A β 42-GLR29 were similar to those observed in A β 42-wt as is shown in Table S2. However, A β 42-GLR33 formed an additional hydrogen bond between Ser26 and Asp23, and A β 42-GLR25 did not form side chain to side chain hydrogen bonds.

The contact map between the A β 42 residues is shown in Figure 8. Regions marked in red indicate residues in close contact (within 0.25 nm of each other), and regions marked in blue stand for residues that display little to no contact. Based on this assignment, one can explain the red main diagonal seen in all contact maps, as it represents the contact of a residue with itself and its neighboring residues. Of interest are those islands of red color that spread in almost all contact maps. Considering the contact map of A β 42-GLR25, these light-orange-colored islands are arranged in cross diagonals between residues 28–34 with residues 14–24, illustrating the formation of β -sheets. Similar diagonals are observed in the other peptides but with some distortion, indicating that no β -sheet formation took place, and to a lesser degree in the following order A β 42-GLR29 > A β 42-GLR33 > A β 42-wt.

2.2.3. The Most Prevalent A β 42 Structures. To substantiate the secondary structure and contact map analysis, we clustered the A β structures using the algorithm developed by Daura et al. The top cluster of each system is presented in Figure 9, while

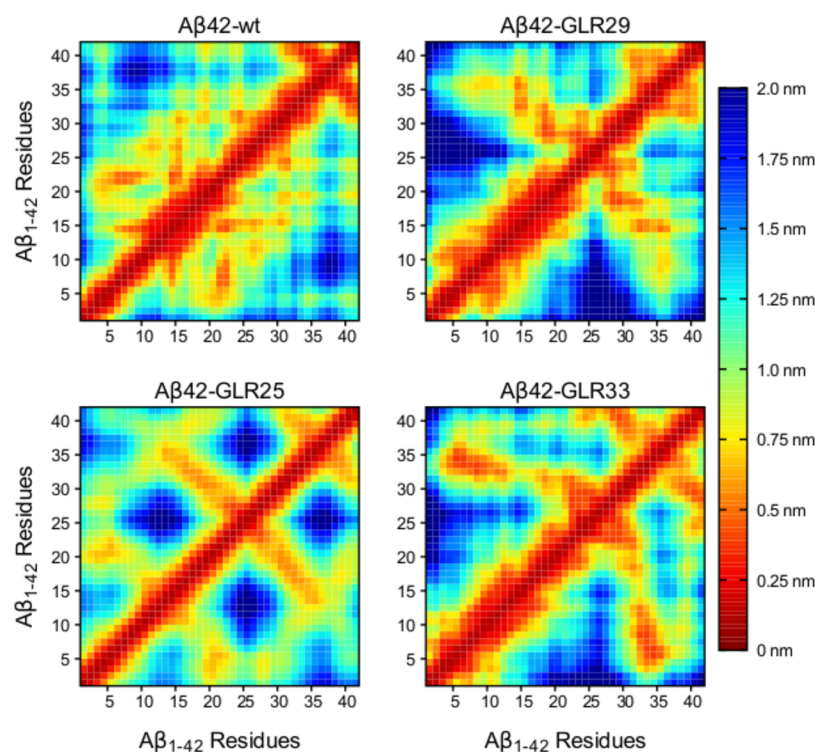


Figure 8. Contact map of each $A\beta_{42}$ residue in the case of $A\beta_{42}$ -wt, $A\beta_{42}$ -GLR25, $A\beta_{42}$ -GLR29, and $A\beta_{42}$ -GLR33 in a bilayer comprised of 70% POPC, 25% CHOL, and 5% GM1. The color box to the right shows the corresponding distance (in nm) to color present in the contact map.

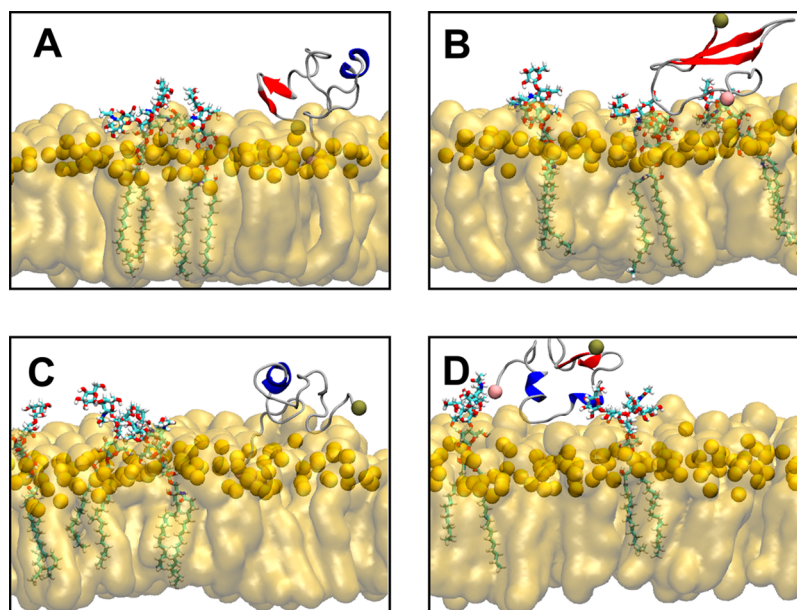


Figure 9. Central structure of the largest cluster: (A) $A\beta_{42}$ -wt (46.7%), (B) $A\beta_{42}$ -GLR25 (33.8%), (C) $A\beta_{42}$ -GLR29 (56.5%), and (D) $A\beta_{42}$ -GLR33 (65.6%). In each rendered image the lipids are colored by orange. The phosphate atom of POPC is in orange, and the N- and C-terminals of $A\beta_{42}$ are shown in pink and tan spheres, respectively. The protein β sheet is shown in red, the helix is shown in blue, and coil and turn are shown in silver.

the structures in the second and third-largest clusters are shown in Figures S6 and S7. The three highest populated $A\beta_{42}$ -wt clusters represented 46.7%, 23.7%, and 9.5% of all structures, respectively (Figure 9A, Figure S6A, and Figure S7A). From the N-terminus to the C-terminus, the secondary structure of the largest and second-largest clusters alternated from random coil to turn, followed by helix at Val12 to Leu17, and then a turn to the antiparallel β -sheet (on either sides of a

turn centered at Gly38) at the C-terminal. There were no β -sheets in the third-largest cluster; however, $A\beta_{42}$ contained coil, turn, and helix. The N-terminus was embedded more deeply into the bilayer in the largest and third-largest clusters and was least embedded in the second-largest cluster. The three most populated structures found in $A\beta_{42}$ -GLR25 represented 33.8%, 18.4%, and 9.4% of all structures, respectively, and are shown in Figure 9B, Figure S6B, and

Figure S7B. The β -sheet structure was observed only in the largest and second-largest clusters; however, a much higher β -sheet content can be seen in these clusters. In addition to the β -sheet at the C-terminal, a β -sheet was observed at the central hydrophobic and polar region (residues Leu17 to Asp23 and Lys28 to Leu34) in the largest cluster and at the metal binding region (Gly9 to Val12) in the second-largest cluster. A helical structure was only observed in the second- and the third-largest clusters. The N-terminus is closer to the bilayer in the largest cluster, while the C-terminus is close to the bilayer in both the second- and third-largest clusters. In the case of A β 42-GLR29, the three representative structures representing 56.5%, 19.3%, and 3.8% of the total number of structures, respectively, are shown in **Figure 9C**, **Figure S6C**, and **Figure S7C**. No β -sheets were observed in any of the three clusters. However, a helical structure was seen in all clusters. Moreover, much more helical content was seen as the helical structure extends to include Glu11 to Glu22 and His13 to Ala21 in the second- and the third-largest clusters, respectively. The N-terminus is embedded in the bilayer in all three clusters, while the C-terminus is only embedded in the second-largest cluster. **Figure 9D**, **Figure S6D**, and **Figure S7D** show the three most populated structures in the presence of A β 42-GLR33, which represent 65.6%, 16%, and 5.2% of the total structures, respectively. In this case the C-terminal β -sheet was observed only in the largest cluster. A helical structure was observed in both the largest and second-largest cluster. There were no helices and no β -sheet in the third-largest cluster. The N-terminus is close to the bilayer in the second-largest cluster, while both the N- and C-terminus residues interact with the solvent in both the largest and the third-largest clusters.

2.3. Discussion. **2.3.1. Effect of Bilayer on A β 42.** The insertion data in **Figure 3**, which shows the time-averaged distance between each A β 42 residue and the bilayer, revealed following order of membrane insertion: A β 42-wt > A β 42-GLR29 > A β 42-GLR25 > A β 42-GLR33. The detailed interactions of A β 42 residues with the bilayer are shown more quantitatively in the peptide-bilayer contacts (**Figure 4**). Interactions between A β 42 and the bilayer occur primarily between the N-terminus and the POPC headgroups, while the remaining residues make more contact with GM1. A β 42-GLR25 makes the least contact with GM1 as the normalized frequency is generally less than 0.5, which can indicate why it has the tendency to adopt the β -sheet conformation while on the membrane surface. As shown in **Figure 4**, the contact between peptides and GM1 is ranked in the order of A β 42-GLR29 > A β 42-GLR33 > A β 42-wt > A β 42-GLR25. Contacts observed at the N-terminus especially with Asp1 and Arg5 were driven by hydrogen bonds that formed between the amino acid residues and the lipids. The propensity of hydrogen bonds to form between A β 42 and GM1 are on the order of A β 42-GLR29 > A β 42-GLR33 > A β 42-GLR25 > A β 42-wt. The hydrogen bond propensity with POPC was limited to residues from the N-terminal metal-binding region, with Asp1 and Arg5 as the main hydrogen bond forming residues. This is expected to be the cause that drives the N-terminus to be close to the bilayer headgroup as can be seen from the insertion data in **Figure 3**. Here, A β 42-wt and A β 42-GLR29 showed a higher hydrogen bond propensity with POPC than A β 42-GLR25 and A β 42-GLR33. It is not surprising that A β 42 residues that form a hydrogen bond with the bilayer were also shown to be the strong energetic contribution to interactions between each peptide and the lipid bilayer. The interactions between each

A β 42 residue and the lipid bilayer were divided into their Coulombic and Lennard-Jones contributions. Overall, it can be seen from **Figures 6** and **S3** that the A β -bilayer interaction is mostly hydrophobic in nature, since most residues interacted with the bilayer via the Lennard-Jones interaction. However, Coulombic interactions played a major role in the case of Asp1 and Arg5 residues in both A β 42-wt and A β 42-GLR29, which is expected due to their tendency to form hydrogen bonds with POPC.

The observation that A β 42 formed the most contacts with GM1 can be attributed to the large headgroup of GM1 containing five sugar groups (**Figure S8**) that tend to lie on the membrane surface, thus providing a platform for hydrogen bonding with A β 42 through its sugar headgroups (**Figure 4**). It should be noted that with 5% GM1 in the bilayer there were only 7 GM1 lipids in each leaflet. Despite this low GM1 content, as can be seen from the most populated clusters (**Figures 9**, **S6**, and **S7**), A β 42 has a preference to bind to GM1 and in some cases even to two GM1 molecules at the same time due to the possibility of hydrogen bonding to the pentasaccharide GM1 headgroup. In order to further elucidate the A β 42-GM1 binding, we dissected these interactions into their contributions per sugar ring. The representative snapshot in **Figure S9** and the contact probability in **Figure S10** show that independent of the oxidation state of A β 42, the peptide made the most contacts with the sugar groups furthest away from the membrane surface, that is the terminal β -D-galactose (Gal'), the N-acetyl- β -D-galactosamine (GalNAc), and the N-acetyl- α -neuraminidate (Neu). Apart from A β 42-GLR25, the other three A β 42 variants preferred binding to Neu, while A β 42-GLR25 formed more contacts with Gal'. The contact probability of A β 42-wt and A β 42-GLR25 with GalNAc is also considerably high, leading to some contacts with the adjacent Gal, while A β 42-GLR29 and A β 42-GLR33 formed only a few contacts with GalNAc. **Figure S11** confirms that in all cases the contacts between A β 42 and the sugar groups are driven by hydrogen-bond formation, which, however, does not only involve Coulomb but also Lennard-Jones interactions (**Figure S12**). The formation of hydrogen bonds of A β 42 with GM1 prevents the peptide from forming intrapeptide hydrogen bonds as needed for secondary structure formation, e.g., the formation of β -sheets and α -helices. This is indeed the case as the numerous snapshots in **Figures 9**, **S6**, and **S7** reveal: at the A β 42-GM1 binding sites, no β -sheet or α -helix is found. However, the binding of A β 42 to GM1 keeps A β 42, or at least parts of it, somewhat above the membrane surface (**Figure 3**), which in turn encourages β -sheet formation as seen for A β 42-GLR25 in **Figure 9B** or helix formation as observed for A β 42-GLR33 in **Figure 9D**. The higher amount of structure formation of membrane-associated A β 42 compared to the solution state can thus be considered to be a consequence of the reduction in conformational flexibility on the membrane surface, while leaving A β 42 enough conformational freedom and also possibilities for intrapeptide hydrogen-bond formation needed for β -sheet or helix formation.

2.3.2. Effect on A β 42 Secondary Structure. The secondary structure of A β 42 has similar secondary structure elements in each system, particularly in the helical central polar region (Val12 to Ala21). This region remained helical in all peptides, though it is extended to include residues Asp7 to Ala21 in A β 42-GLR33. As evidenced by the membrane contacts, hydrogen bonding, and interaction energies, the conformation of A β 42 in the N-terminal region was not affected by the

interaction with POPC. This is because A β 42-GLR25 showed higher contact frequency with POPC in the N-terminal compared to A β 42-GLR33; however, both peptides showed no tendency to form β -sheets in the N-terminal region. The same is applied to A β 42-GLR29 and A β 42-wt. On the other hand, the interaction with GM1 affected the formation of β -sheets. It was observed that A β 42-GLR29 and A β 42-GLR33 showed the highest number of contacts with GM1 when compared to A β 42-wt and A β 42-GLR25, but these peptides had a lower tendency to form β -sheets, which is in agreement with the finding of Mandel et al. on A β 40.⁷³ This is also confirmed by the insertion data (Figure 3) which shows that A β 42-wt and A β 42-GLR25 behave differently with respect to the bilayer, with both peptides having a lower tendency to bind to GM1 (Figure 4) than A β 42-GLR29 and A β 42-GLR33 do.

The assignment of the secondary structure is shown in Figure 7, and it mirrors what is seen in the most populated clusters as shown in Figure 9. The intrapeptide backbone hydrogen bonds indicate a structure that is very similar to that of a β -sheet in the most populated clusters for these two systems.

2.3.3. Comparison with Other Studies. It is known from experimental findings and MD simulations that A β 42 is an intrinsically disordered protein, containing all possible secondary structures.^{9,74–77} It has also been shown that the C-terminal β -sheet is the seed for further A β aggregation into a β -sheet rich structure.⁷⁴ Moreover, the importance of the total β -strand content for controlling the aggregation rates was pointed out in an MD study by Man et al.⁷⁸ In our study we observed a C-terminal β -sheet in the case of A β 42-wt and A β 42-GLR25 especially in two regions, Val39-Ile41 and Ala30-Val36. We also found that there is a β -sheet forming propensity in the regions of Leu17 to Glu22 and Tyr10 to Glu11 in A β 42-GLR25. However, the β -sheet forming propensity in the C-terminal hydrophobic region was very low in the cases of A β 42-GLR29 and A β 42-GLR33, which might be explained by the findings of Fonte et al.⁵³ and Harmeier et al.⁵⁴ Fonte et al. found experimentally that changes in the glycine zipper Gly29-XXX-Gly33-XXX-Gly37 motif prevent the formation of toxic oligomers as they observed a reduction in A β toxicity upon the substitution of Gly37 with leucine.⁵³ It was also found by Harmeier et al. that the substitution of Gly33, which is both at the end of one and at the start of the next GXXXG interaction motif, causes the formation of less toxic oligomers. Based on that, we suggest that the stability of the C-terminal β -sheet in A β 42-GLR25 might be attributed to the fact that Gly25 does not disrupt the zipper motif.

According to our findings, the effect of radicalization of the Gly residue on the structure of A β 42 depends on the position of the oxidized Gly residue within the C-terminal hydrophobic region of A β . This is supported by the MD study of Owen and co-workers on three fast folding miniproteins, where it was also found that the denaturing effect of the Gly radicals depended on the position of the radical.⁶⁴ Structural changes in the protein upon Gly oxidation were more pronounced in the α -helix rich protein than in the β -sheet rich one due to the flat geometry of the radical (Figure S1).⁶⁴ This may even cause the formation of a β -sheet as Owen et al. showed in an MD study of a short helical peptide that underwent a transition to a β -sheet conformation upon radical formation.⁶³

It has been shown experimentally that A β interacts strongly with lipid bilayers comprised of phosphatidylcholine headgroups.^{79,80} In our study we found that this interaction is

mediated by hydrogen bonds with the positively charged N-terminal Asp1 and the side chain of Arg5. Furthermore, we found that such tight interactions have no effect on the A β secondary structure, which is in agreement with the experimental findings that binding of A β to PC-containing bilayers does not affect the secondary structure of the A β peptide at low concentrations.^{81,82} Our results showed how the bulky GM1 headgroups cover a large area of the membrane even with only 7 GM1 lipids in each bilayer leaflet, and the peptide is more likely to bind to the GM1 headgroups, especially to the terminal saccharide residues, than to the POPC headgroups. This agrees with the findings by Manna et al., who concluded that the GM1 headgroups act as a scaffold for A β binding through sugar-specific interactions.⁸³ They further observed the formation of a C-terminal β -hairpin upon binding of A β 42 to GM1, which is also in line with our results. However, it should be noted that another study found that the binding of A β 40 to GM1 headgroups induces the formation of a helix on the C-terminal side of the peptide.⁸⁴ We also observed helix formation upon GM1 binding, which, however, occurred preferentially between residues 10 and 21 of A β 42. This includes the region from 17 to 21 that was already identified as helical for A β 40 in solution.⁸⁵ From an experimental study it was followed that low concentrations of GM1, i.e., physiological concentration of GM1 that ranged from 2–4% of the total lipid content of the membrane,⁸⁶ enhance the formation of β -sheets but prevent A β oligomerization.⁸⁷ Other experiments further showed that the higher the concentrations of GM1 (but less physiologically relevant), the higher the β -sheet content of A β becomes.⁸⁸

3. CONCLUSION

Understanding the interplay between oxidative stress and A β neurotoxicity requires exploring the conformation of oxidized A β peptides. Based on our MD simulations of A β 42 and its oxidized variants in interplay with a model membrane bilayer, we found that A β 42-GLR25 is potentially as toxic as A β 42-wt, assuming that β -sheet formation in A β is connected to its toxicity,¹² whereas A β 42-GLR29 and A β 42-GLR33 showed less β -sheet forming propensity. We also revealed that the sugar moiety of GM1 affects the interaction between A β 42 and the membrane. A β has a high tendency to interact with GM1 (especially A β 42-GLR29 and A β 42-GLR33), and once this happens the propensity of the peptide to form β -sheet is greatly reduced as A β , instead of forming intrapeptide hydrogen bonds, interacts with GM1 through hydrogen bonds. Moreover, the interaction with GM1 also reduces the number of contacts and hydrogen bonds that the peptide makes with POPC. On the other hand, the insertion of the peptide into the bilayer is enhanced by its interaction with POPC; A β 42-wt and A β 42-GLR29 showed the highest number of contacts with POPC, and therefore these peptides interact most closely with the bilayer. Our results suggest that the differences observed in A β conformation and interaction with the bilayer upon the oxidation of different glycine residues might be attributed in part to the position of these residues within the C-terminal hydrophobic region of A β and its subsequent interaction with GM1. Further studies should test this observation and further determine the role of oxidation in A β -mediated AD toxicity.

4. METHODS

4.1. Model System and System Equilibration. The starting structures for the wild-type (wt) and oxidized (Gly25, Gly29, Gly33) $A\beta$ peptides were obtained from 1 μ s simulations, using the final snapshots of these simulations (Figure S13). These simulations had begun with the structure of $A\beta$ 42 as determined by NMR spectroscopy (PDB ID: 1Z0Q).⁸⁹ The N- and C-terminals were the free amino (NH_3^+) and carboxyl (COO^-) groups, respectively, and thus each peptide carried an overall charge of -3 . The oxidized $A\beta$ 42 peptides will be henceforth referred to as $A\beta$ 42-GLR25, $A\beta$ 42-GLR29, and $A\beta$ 42-GLR33. The four peptides were placed 3.5 nm above a symmetric membrane composed of 202 POPC, 72 CHOL, and 14 GM1 lipids. Each system was solvated with the TIP3P water model⁹⁰ and neutralized with 17 Na^+ ions. In addition, 150 mM NaCl was added to mimic the physiological concentration of these ions. The exact numbers of each molecule present in each system are listed in Table 1. All interactions among system constituents were described using OPLS-AA force field parameters.^{66,91–93} All MD simulations were carried out using the GROMACS 4.6 simulation package.⁹⁴

Table 1. Molecular Composition of the Four Membrane Systems: $A\beta$ 42-wt, $A\beta$ 42-GLR25, $A\beta$ 42-GLR29, and $A\beta$ 42-GLR33

bilayer system	number of molecules						
	peptide	lipids			ions		water
		$A\beta$ 42	POPC	CHOL	GM1	Na^+	
$A\beta$ 42-wt	1	202	72	14	69	52	19301
$A\beta$ 42-GLR25	1	202	72	14	69	52	19289
$A\beta$ 42-GLR29	1	202	72	14	69	52	19293
$A\beta$ 42-GLR33	1	202	72	14	69	52	19259

The systems were energy minimized using the steepest descent algorithm to remove all atomic clashes.^{95,96} This was followed by an equilibration under NVT conditions for 1 ns, where the reference temperature of 310 K was regulated with the velocity-rescale thermostat⁹⁷ and the time constant was set to 0.1 ps. During minimization and initial equilibration stages, the heavy atoms of protein and lipids were subjected to position restraints with a force constant of 1000 kJ/mol·nm². Next, the system was equilibrated under NPT conditions for 10 ns to obtain a pressure of 1.0 bar. The pressure was regulated using a semi-isotropic Parrinello–Rahman pressure coupling scheme^{98–100} with a time constant of 5 ps and isothermal compressibility of 4.5e-5 bar⁻¹. The temperature of 310 K was maintained with a Nosé–Hoover thermostat^{101–104} with a time constant of 0.5 ps, while the position restraints on the protein and lipids were still on. The particle Mesh Ewald (PME)^{105,106} method was used to account for the electrostatic interactions within the system. Both the short-range interactions, with a van der Waals cutoff of 1.0 nm (real space), and the long-range (Fourier) electrostatics were used under the periodicity assumption, and the periodic boundary conditions were set in all directions. All bonds were constrained using the LINCS algorithm.¹⁰⁷

4.2. Hamiltonian Replica Exchange MD (HREMD) Simulations. For the final production run, the input parameters were the same as those under NPT conditions, except that the position restraints were switched off. To accelerate conformational sampling, we employed the HREMD protocol for the systems described in the previous section using the protocol introduced in ref 108. System coordinates and input parameters (without restraints) from the NPT equilibration served as the initial input to generate the postprocessed topology files required for the HREMD simulations. The system was split into hot ($A\beta$ peptide) and cold (the rest of the system) regions, where the interactions within the hot region and between the hot region and the cold region were enhanced by scaling the force field terms for the proper dihedrals, Lennard-Jones parameters, and electrostatic interactions. HREMD simulations were performed using 14 replicas with λ values ranging from 1 to 0.5, and replica

exchanges were attempted every 2 ps. Each system was simulated for 200 ns per λ value with the average exchange acceptance ratio of 0.13. All simulations were carried out with GROMACS 4.6 patched to PLUMED 2.2.¹⁰⁹

4.3. Analysis Methods. **4.3.1. Bilayer-Peptide Interactions.** The analysis of each system began when $A\beta$ was within 0.5 nm of the bilayer. All analysis programs mentioned in this section are included in the GROMACS 2018.2 program package.^{110–113} The “gmxtraj” program was used to measure the insertion distance of $A\beta$ 42 by computing the center of mass (COM) of each residue, and the average vertical position of the phosphorus atoms of phospholipids was taken along the z-axis. The “gmxtmindist” program was employed to determine the number of contacts between each $A\beta$ 42 residue and each POPC or GM1 lipid. A contact was recorded when the distance between any two non-hydrogen atoms from the residue and lipid in question was within 0.5 nm. Then the number of contacts was normalized in the range of 0 to 1. The hydrogen bond propensity was determined by the number of times a hydrogen bond was formed between hydrogen bond donating and accepting atoms in $A\beta$ 42 and each lipid type using the “gmxt hbond” program. A hydrogen bond was recorded when the angle between the donor and acceptor bonded hydrogen was between 150 and 180 deg and the distance between the two atoms was within 0.35 nm. The “gmxt energy” program was used to calculate the interactions energy between each $A\beta$ residue and the headgroup of POPC or GM1.

4.3.2. $A\beta$ 42 Structure. The secondary structure of each $A\beta$ 42 residue was determined using the *define secondary structure program* (do_dssp).¹¹⁴ To facilitate a clear representation, the data of similar secondary structures are grouped together; β -strand and β -bridge are combined as β -strand/bridge, β -turn and bend are combined as β -turn/bend, and helix includes α , π , and 3_{10} helices. Hydrogen bonds within the peptide backbone, between the backbone and side chains, and between the side chains were counted by applying the same method used for counting the peptide-lipid hydrogen bonds. Representative $A\beta$ 42 structures were obtained by the “gmxt cluster” program using the method of Daura et al.¹¹⁵ and a cutoff of 0.25 nm for clustering. The conformation and membrane interactions of the central structure of the three largest clusters were rendered using the VMD program.¹¹⁶

■ ASSOCIATED CONTENT

Supporting Information

The Supporting Information is available free of charge at <https://pubs.acs.org/doi/10.1021/acschemneuro.9b00558>.

Figures and tables explaining structure used in study and enhancing analysis (PDF)

■ AUTHOR INFORMATION

Corresponding Author

Michael C. Owen – CEITEC – Central European Institute of Technology, Masaryk University, Brno 625 00, Czech Republic; orcid.org/0000-0001-9076-7114; Email: michaelowen27@gmail.com

Authors

Hebah Fatafta – Institute of Biological Information Processing (IBI-7: Structural Biochemistry), Forschungszentrum Jülich, 52425 Jülich, Germany

Chetan Poojari – Department of Physics, University of Helsinki, FI-00014 Helsinki, Finland; Theoretical Physics and Center for Biophysics, Saarland University, 66123 Saarbrücken, Germany

Abdallah Sayyed-Ahmad – Department of Physics, Birzeit University, Birzeit 71939, Palestine; orcid.org/0000-0003-2415-8403

Birgit Strodel – Institute of Biological Information Processing (IBI-7: Structural Biochemistry), Forschungszentrum Jülich,

52425 Jülich, Germany; Institute of Theoretical and Computational Chemistry, Heinrich Heine University Düsseldorf, 40225 Düsseldorf, Germany; orcid.org/0000-0002-8734-7765

Complete contact information is available at:
<https://pubs.acs.org/10.1021/acscchemneuro.9b00558>

Author Contributions

All authors made a significant contribution to this manuscript. The contribution of each author is as follows: H.F. analyzed simulation data, prepared figures, presented data, and wrote the manuscript. C.P. designed the study, set up simulations, and wrote the manuscript. A.S.-A. provided study funding and wrote the manuscript. B.S. provided study funding, interpreted simulation data, and wrote the manuscript. M.C.O. designed the study, provided study funding, carried out simulations, and wrote the manuscript.

Notes

This article reflects only the author's (M.C.O.) view, and the EU is not responsible for any use that may be made of the information it contains.

The authors declare no competing financial interest.

ACKNOWLEDGMENTS

H.F., A.S.-A., and B.S. acknowledge funding for this project from the Palestinian-German Science Bridge financed by the German Federal Ministry of Education and Research (BMBF). H.F. and B.S. gratefully acknowledge the computing time granted through JARA-HPC (project JICS6C) on the supercomputer JURECA at Forschungszentrum Jülich. This project has received funding from the European Union's Horizon 2020 research and innovation programme under the Marie Skłodowska-Curie grant agreement no. 665860, and it is cofinanced by the South Moravian Region. M.C.O. also thanks the Helmholtz Postdoc Programme. Access to computing and storage facilities owned by parties and projects contributing to the National Grid Infrastructure MetaCentrum provided under the programme "Projects of Large Research, Development, and Innovations Infrastructures" (CESNET LM2015042) is greatly appreciated.

REFERENCES

- (1) Burns, A., and Iliffe, S. (2009) Alzheimer's disease. *Br. Med. J.* 338, 467–471.
- (2) Förstl, H., and Kurz, A. (1999) Clinical features of Alzheimer's disease. *Eur. Arch. Psy. Clin. N.* 249, 288–290.
- (3) Niu, Z., Zhang, Z., Zhao, W., and Yang, J. (2018) Interactions between amyloid β peptide and lipid membranes. *Biochim. Biophys. Acta, Biomembr.* 1860, 1663–1669.
- (4) Rangachari, V., Dean, D. N., Rana, P., Vaidya, A., and Ghosh, P. (2018) Cause and consequence of $A\beta$ -Lipid interactions in Alzheimer disease pathogenesis. *Biochim. Biophys. Acta, Biomembr.* 1860, 1652–1662.
- (5) Cheng, Q., Hu, Z.-W., Doherty, K. E., Tobin-Miyaji, Y. J., and Qiang, W. (2018) The on-fibrillation-pathway membrane content leakage and off-fibrillation-pathway lipid mixing induced by 40-residue β -amyloid peptides in biologically relevant model liposomes. *Biochim. Biophys. Acta, Biomembr.* 1860, 1670–1680.
- (6) Owen, M. C., Gnutz, D., Gao, M., Wärländer, S. K., Jarvet, J., Gräslund, A., Winter, R., Ebbinghaus, S., and Strodel, B. (2019) Effects of in vivo conditions on amyloid aggregation. *Chem. Soc. Rev.* 48, 3946–3996.
- (7) Hardy, J. A., and Higgins, G. A. (1992) Alzheimer's disease: the amyloid cascade hypothesis. *Science* 256, 184–186.
- (8) Cheng, R. P., Gellman, S. H., and DeGrado, W. F. (2001) β -Peptides: from structure to function. *Chem. Rev.* 101, 3219–3232.
- (9) Lührs, T., Ritter, C., Adrian, M., Riek-Loher, D., Bohrmann, B., Döbeli, H., Schubert, D., and Riek, R. (2005) 3D structure of Alzheimer's amyloid- β (1–42) fibrils. *Proc. Natl. Acad. Sci. U. S. A.* 102, 17342–17347.
- (10) Kael, M. A., Weber, D. K., Separovic, F., and Sani, M.-A. (2018) Aggregation kinetics in the presence of brain lipids of $A\beta$ (1–40) cleaved from a soluble fusion protein. *Biochim. Biophys. Acta, Biomembr.* 1860, 1681–1686.
- (11) Marshall, K. E., Vadukul, D. M., Dahal, L., Theisen, A., Fowler, M. W., Al-Hilaly, Y., Ford, L., Kemeses, G., Day, I. J., Staras, K., and Serpell, L. C. (2016) A critical role for the self-assembly of Amyloid- β 1–42 in neurodegeneration. *Sci. Rep.* 6, 30182.
- (12) Ono, K., Condrón, M. M., and Teplow, D. B. (2009) Structure–neurotoxicity relationships of amyloid β -protein oligomers. *Proc. Natl. Acad. Sci. U. S. A.* 106, 14745–14750.
- (13) El-Agnaf, O. M., Mahil, D. S., Patel, B. P., and Austen, B. M. (2000) Oligomerization and toxicity of β -amyloid-42 implicated in Alzheimer's disease. *Biochem. Biophys. Res. Commun.* 273, 1003–1007.
- (14) Petkova, A. T., Ishii, Y., Balbach, J. J., Antzutkin, O. N., Leapman, R. D., Delaglio, F., and Tycko, R. (2002) A structural model for Alzheimer's β -amyloid fibrils based on experimental constraints from solid state NMR. *Proc. Natl. Acad. Sci. U. S. A.* 99, 16742–16747.
- (15) Kim, W., and Hecht, M. H. (2006) Generic hydrophobic residues are sufficient to promote aggregation of the Alzheimer's $A\beta$ 42 peptide. *Proc. Natl. Acad. Sci. U. S. A.* 103, 15824–15829.
- (16) Cukalevski, R., Boland, B., Frohm, B., Thulin, E., Walsh, D., and Linse, S. (2012) Role of aromatic side chains in amyloid β -protein aggregation. *ACS Chem. Neurosci.* 3, 1008–1016.
- (17) Poojari, C., Kukol, A., and Strodel, B. (2013) How the amyloid- β peptide and membranes affect each other: An extensive simulation study. *Biochim. Biophys. Acta, Biomembr.* 1828, 327–339.
- (18) Poojari, C., and Strodel, B. (2013) Stability of transmembrane amyloid β -peptide and membrane integrity tested by molecular modeling of site-specific $A\beta$ 42 mutations. *PLoS One* 8, e78399.
- (19) Varadarajan, S., Yatin, S., Aksenova, M., and Butterfield, D. A. (2000) Alzheimer's amyloid β -peptide-associated free radical oxidative stress and neurotoxicity. *J. Struct. Biol.* 130, 184–208.
- (20) Butterfield, D. A., and Lauderback, C. M. (2002) Lipid peroxidation and protein oxidation in Alzheimer's disease brain: potential causes and consequences involving amyloid β -peptide-associated free radical oxidative stress. *Free Radical Biol. Med.* 32, 1050–1060.
- (21) Drake, J., Link, C. D., and Butterfield, D. A. (2003) Oxidative stress precedes fibrillar deposition of Alzheimer's disease amyloid β -peptide (1–42) in a transgenic *Caenorhabditis elegans* model. *Neurobiol. Aging* 24, 415–420.
- (22) Butterfield, D. A. (2004) Proteomics: a new approach to investigate oxidative stress in Alzheimer's disease brain. *Brain Res.* 1000, 1–7.
- (23) Sultana, R., and Butterfield, D. A. (2010) Role of oxidative stress in the progression of Alzheimer's disease. *J. Alzheimer's Dis.* 19, 341–353.
- (24) Huang, W.-J., Zhang, X., and Chen, W.-W. (2016) Role of oxidative stress in Alzheimer's disease. *Biomed. Rep.* 4, 519–522.
- (25) Brown, D. R. (2005) Neurodegeneration and oxidative stress: prion disease results from loss of antioxidant defence. *Folia Neuropathol.* 43, 229–243.
- (26) Cheignon, C., Tomas, M., Bonnefont-Rousselot, D., Faller, P., Hureau, C., and Collin, F. (2018) Oxidative stress and the amyloid beta peptide in Alzheimer's disease. *Redox Biol.* 14, 450–464.
- (27) Smith, D. G., Cappai, R., and Barnham, K. J. (2007) The redox chemistry of the Alzheimer's disease amyloid β peptide. *Biochim. Biophys. Acta, Biomembr.* 1768, 1976–1990.
- (28) Zhao, Y., and Zhao, B. (2013) Oxidative stress and the pathogenesis of Alzheimer's disease. *Oxid. Med. Cell. Longevity* 2013 (2013), 316523.

- (29) Minicozzi, V., Stellato, F., Comai, M., Dalla Serra, M., Potrich, C., Meyer-Klaucke, W., and Morante, S. (2008) Identifying the minimal copper- and zinc-binding site sequence in amyloid- β peptides. *J. Biol. Chem.* 283, 10784–10792.
- (30) Marino, T., Russo, N., Toscano, M., and Pavelka, M. (2010) On the metal ion (Zn^{2+} , Cu^{2+}) coordination with beta-amyloid peptide: DFT computational study. *Interdiscip. Sci.: Comput. Life Sci.* 2, 57–69.
- (31) Roberts, B. R., Ryan, T. M., Bush, A. I., Masters, C. L., and Duce, J. A. (2012) The role of metallobiology and amyloid- β peptides in Alzheimer's disease. *J. Neurochem.* 120, 149–166.
- (32) Pearson, H. A., and Peers, C. (2006) Physiological roles for amyloid β peptides. *J. Physiol. (Oxford, U. K.)* 575, 5–10.
- (33) Brothers, H. M., Gosztyla, M. L., and Robinson, S. R. (2018) The Physiological Roles of Amyloid- β Peptide Hint at New Ways to Treat Alzheimer's Disease. *Front. Aging Neurosci.* 10, 118.
- (34) Michikawa, M., Gong, J.-S., Fan, Q.-W., Sawamura, N., and Yanagisawa, K. (2001) A novel action of Alzheimer's amyloid β -protein ($A\beta$): oligomeric $A\beta$ promotes lipid release. *J. Neurosci.* 21, 7226–7235.
- (35) Koudinova, N. V., Koudinov, A. R., and Yavin, E. (2000) Alzheimer's $A\beta$ 1–40 Peptide Modulates Lipid Synthesis in Neuronal Cultures and Intact Rat Fetal Brain Under Normoxic and Oxidative Stress Conditions. *Neurochem. Res.* 25, 653–660.
- (36) Yanagisawa, K., Odaka, A., Suzuki, N., and Ihara, Y. (1995) GM1 ganglioside-bound amyloid β -protein ($A\beta$): A possible form of preamyloid in Alzheimer's disease. *Nat. Med. (N. Y., NY, U. S.)* 1, 1062.
- (37) Di Scala, C., Chahinian, H., Yahi, N., Garmy, N., and Fantini, J. (2014) Interaction of Alzheimer's β -amyloid peptides with cholesterol: mechanistic insights into amyloid pore formation. *Biochemistry* 53, 4489–4502.
- (38) Kakio, A., Nishimoto, S.-i., Yanagisawa, K., Kozutsumi, Y., and Matsuzaki, K. (2002) Interactions of amyloid β -protein with various gangliosides in raft-like membranes: importance of GM1 ganglioside-bound form as an endogenous seed for Alzheimer amyloid. *Biochemistry* 41, 7385–7390.
- (39) Thomaier, M., Gremer, L., Dammers, C., Fabig, J., Neudecker, P., and Willbold, D. (2016) High-affinity binding of monomeric but not oligomeric amyloid- β to ganglioside GM1 containing nanodiscs. *Biochemistry* 55, 6662–6672.
- (40) Di Scala, C., Yahi, N., Boutemur, S., Flores, A., Rodriguez, L., Chahinian, H., and Fantini, J. (2016) Common molecular mechanism of amyloid pore formation by Alzheimer's β -amyloid peptide and α -synuclein. *Sci. Rep.* 6, 28781.
- (41) Eckert, G. P., Kirsch, C., Leutz, S., Wood, W. G., and Müller, W. E. (2003) Cholesterol modulates amyloid beta-peptide's membrane interactions. *Pharmacopsychiatry* 36, 136–143.
- (42) Fantini, J., Yahi, N., and Garmy, N. (2013) Cholesterol accelerates the binding of Alzheimer's β -amyloid peptide to ganglioside GM1 through a universal hydrogen-bond-dependent sterol tuning of glycolipid conformation. *Front. Physiol.* 4, 120.
- (43) Cui, Z. J., Han, Z. Q., and Li, Z. Y. (2012) Modulating protein activity and cellular function by methionine residue oxidation. *Amino Acids* 43, 505–517.
- (44) Butterfield, D. A., and Kanski, J. (2002) Methionine residue 35 is critical for the oxidative stress and neurotoxic properties of Alzheimer's amyloid β -peptide 1–42. *Peptides* 23, 1299–1309.
- (45) Butterfield, D. A., and Boyd-Kimball, D. (2005) The critical role of methionine 35 in Alzheimer's amyloid β -peptide (1–42)-induced oxidative stress and neurotoxicity. *Biochim. Biophys. Acta, Proteins Proteomics* 1703, 149–156.
- (46) Butterfield, D. A., and Sultana, R. (2011) Methionine-35 of $A\beta$ (1–42): importance for oxidative stress in Alzheimer disease. *J. Amino Acids* 2011, 198430.
- (47) Boyd-Kimball, D., Sultana, R., Mohammad-Abdul, H., and Butterfield, D. A. (2005) Neurotoxicity and oxidative stress in DIM-substituted Alzheimer's $A\beta$ (1–42): relevance to N-terminal methionine chemistry in small model peptides. *Peptides* 26, 665–673.
- (48) Varadarajan, S., Kanski, J., Aksenova, M., Lauderback, C., and Butterfield, D. A. (2001) Different Mechanisms of Oxidative Stress and Neurotoxicity for Alzheimer's $A\beta$ (1–42) and $A\beta$ (25–35). *J. Am. Chem. Soc.* 123, 5625–5631.
- (49) Varadarajan, S., Yatin, S., Kanski, J., Jahanshahi, F., and Butterfield, D. A. (1999) Methionine residue 35 is important in amyloid β -peptide-associated free radical oxidative stress. *Brain Res. Bull.* 50, 133–141.
- (50) Kanski, J., Varadarajan, S., Aksenova, M., and Butterfield, D. A. (2002) Role of glycine-33 and methionine-35 in Alzheimer's amyloid β -peptide 1–42-associated oxidative stress and neurotoxicity. *Biochim. Biophys. Acta, Mol. Basis Dis.* 1586, 190–198.
- (51) Rauk, A., Armstrong, D. A., and Fairlie, D. P. (2000) Is oxidative damage by β -amyloid and prion peptides mediated by hydrogen atom transfer from glycine α -carbon to methionine sulfur within β -sheets? *J. Am. Chem. Soc.* 122, 9761–9767.
- (52) Mazzitelli, S., Filippello, F., Rasile, M., Lauranzano, E., Starvaggi-Cucuzza, C., Tamborini, M., Pozzi, D., Barajon, I., Giorgino, T., Natalello, A., and Matteoli, M. (2016) Amyloid- β 1–24 C-terminal truncated fragment promotes amyloid- β 1–42 aggregate formation in the healthy brain. *Acta Neuropathol. Commun.* 4, 110.
- (53) Fonte, V., Dostal, V., Roberts, C. M., Gonzales, P., Lacor, P., Magrane, J., Dingwell, N., Fan, E. Y., Silverman, M. A., Stein, G. H., and Link, C. D. (2011) A glycine zipper motif mediates the formation of toxic β -amyloid oligomers in vitro and in vivo. *Mol. Neurodegener.* 6, 61.
- (54) Harmeier, A., Wozny, C., Rost, B. R., Munter, L.-M., Hua, H., Georgiev, O., Beyermann, M., Hildebrand, P. W., Weise, C., Schaffner, W., and Schmitz, D. (2009) Role of amyloid- β glycine 33 in oligomerization, toxicity, and neuronal plasticity. *J. Neurosci.* 29, 7582–7590.
- (55) Stuyver, T., Danovich, D., and Shaik, S. (2019) Captodative Substitution Enhances the Diradical Character of Compounds, Reduces Aromaticity, and Controls Single-Molecule Conductivity Patterns: A Valence Bond Study. *J. Phys. Chem. A* 123, 7133–7141.
- (56) Viehe, H. G., Janousek, Z., Merenyi, R., and Stella, L. (1985) The captodative effect. *Acc. Chem. Res.* 18, 148–154.
- (57) Green, M. C., Stelzleni, S., and Francisco, J. S. (2013) Spectral Marker for C α Damage in Beta Peptides. *J. Phys. Chem. A* 117, 550–565.
- (58) Davies, M. J. (2005) The oxidative environment and protein damage. *Biochim. Biophys. Acta, Proteins Proteomics* 1703, 93–109.
- (59) Song, Y., Li, P., Liu, L., Bortolini, C., and Dong, M. (2018) Nanostructural Differentiation and Toxicity of Amyloid- β 25–35 Aggregates Emerge from Distinct Secondary Conformation. *Sci. Rep.* 8, 765.
- (60) Hughes, E., Burke, R. M., and Doig, A. J. (2000) Inhibition of Toxicity in the β -Amyloid Peptide Fragment β -(25–35) Using N-Methylated Derivatives A GENERAL STRATEGY TO PREVENT AMYLOID FORMATION. *J. Biol. Chem.* 275, 25109–25115.
- (61) Karplus, M., and McCammon, J. A. (2002) Molecular dynamics simulations of biomolecules. *Nat. Struct. Biol.* 9, 646.
- (62) Dror, R. O., Jensen, M. Ø., Borhani, D. W., and Shaw, D. E. (2010) Exploring atomic resolution physiology on a femtosecond to millisecond timescale using molecular dynamics simulations. *J. Gen. Physiol.* 135, 555–562.
- (63) Owen, M. C., Strodel, B., Csizmadia, I. G., and Viskolcz, B. (2016) Radical formation initiates solvent-dependent unfolding and β -sheet formation in a model helical peptide. *J. Phys. Chem. B* 120, 4878–4889.
- (64) Owen, M. C., Csizmadia, I. G., Viskolcz, B., and Strodel, B. (2017) Protein stability and unfolding following glycine radical formation. *Molecules* 22, 655.
- (65) Liao, Q., Owen, M. C., Bali, S., Barz, B., and Strodel, B. (2018) $A\beta$ under stress: the effects of acidosis, Cu^{2+} -binding, and oxidation on amyloid β -peptide dimers. *Chem. Commun. (Cambridge, U. K.)* 54, 7766–7769.

- (66) Komáromi, I., Owen, M. C., Murphy, R. F., and Lovas, S. (2008) Development of glycol radical parameters for the OPLS-AA/L force field. *J. Comput. Chem.* 29, 1999–2009.
- (67) Meli, M., and Colombo, G. (2013) A Hamiltonian replica exchange molecular dynamics (MD) method for the study of folding, based on the analysis of the stabilization determinants of proteins. *Int. J. Mol. Sci.* 14, 12157–12169.
- (68) Allen, W. J., Lemkul, J. A., and Bevan, D. R. (2009) GridMAT-MD: a grid-based membrane analysis tool for use with molecular dynamics. *J. Comput. Chem.* 30, 1952–1958.
- (69) Gapsys, V., de Groot, B. L., and Briones, R. (2013) Computational analysis of local membrane properties. *J. Comput.-Aided Mol. Des.* 27, 845–858.
- (70) Persson, F., Söderhjelm, P., and Halle, B. (2018) The geometry of protein hydration. *J. Chem. Phys.* 148, 215101.
- (71) Fox, S. J., Lakshminarayanan, R., Beuerman, R. W., Li, J., and Verma, C. S. (2018) Conformational Transitions of Melittin between Aqueous and Lipid Phases: Comparison of Simulations with Experiments. *J. Phys. Chem. B* 122, 8698–8705.
- (72) Matthes, D., and De Groot, B. L. (2009) Secondary structure propensities in peptide folding simulations: a systematic comparison of molecular mechanics interaction schemes. *Biophys. J.* 97, 599–608.
- (73) Mandal, P. K., and Pettegrew, J. W. (2004) Alzheimer's disease: NMR studies of asialo (GM1) and trisialo (GT1b) ganglioside interactions with A β (1–40) peptide in a membrane mimic environment. *Neurochem. Res.* 29, 447–453.
- (74) Rosenman, D. J., Connors, C. R., Chen, W., Wang, C., and García, A. E. (2013) A β monomers transiently sample oligomer and fibril-like configurations: Ensemble characterization using a combined MD/NMR approach. *J. Mol. Biol.* 425, 3338–3359.
- (75) Fawzi, N. L., Phillips, A. H., Ruscio, J. Z., Doucleff, M., Wemmer, D. E., and Head-Gordon, T. (2008) Structure and dynamics of the A β 21–30 peptide from the interplay of NMR experiments and molecular simulations. *J. Am. Chem. Soc.* 130, 6145–6158.
- (76) Carballo-Pacheco, M., and Strodel, B. (2017) Comparison of force fields for Alzheimer's A: A case study for intrinsically disordered proteins. *Protein Sci.* 26, 174–185.
- (77) Nasica-Labouze, J., Nguyen, P. H., Sterpone, F., Berthoumieu, O., Buchete, N.-V., Cote, S., De Simone, A., Doig, A. J., Faller, P., Garcia, A., and Laio, A. (2015) Amyloid β protein and Alzheimer's disease: When computer simulations complement experimental studies. *Chem. Rev. (Washington, DC, U. S.)* 115, 3518–3563.
- (78) Man, V. H., He, X., Derreumaux, P., Ji, B., Xie, X.-Q., Nguyen, P. H., and Wang, J. (2019) Effects of All-Atom Molecular Mechanics Force Fields on Amyloid Peptide Assembly: The Case of A β 16–22 Dimer. *J. Chem. Theory Comput.* 15, 1440–1452.
- (79) Ding, H., Schauerte, J. A., Steel, D. G., and Gafni, A. (2012) β -amyloid (1–40) peptide interactions with supported phospholipid membranes: A single-molecule study. *Biophys. J.* 103, 1500–1509.
- (80) Korshavn, K. J., Satriano, C., Lin, Y., Zhang, R., Dulchavsky, M., Bhunia, A., Ivanova, M. I., Lee, Y.-H., La Rosa, C., Lim, M. H., and Ramamoorthy, A. (2017) Reduced lipid bilayer thickness regulates the aggregation and cytotoxicity of amyloid- β . *J. Biol. Chem.* 292, 4638–4650.
- (81) Qiang, W., Yau, W.-M., and Schulte, J. (2015) Fibrillation of β amyloid peptides in the presence of phospholipid bilayers and the consequent membrane disruption. *Biochim. Biophys. Acta, Biomembr.* 1848, 266–276.
- (82) Terzi, E., Hölzemann, G., and Seelig, J. (1995) Self-association of β -amyloid peptide (1–40) in solution and binding to lipid membranes. *J. Mol. Biol.* 252, 633–642.
- (83) Manna, M., and Mukhopadhyay, C. (2013) Binding, conformational transition and dimerization of amyloid- β peptide on GM1-containing ternary membrane: insights from molecular dynamics simulation. *PLoS One* 8, e71308.
- (84) Tachi, Y., Okamoto, Y., and Okumura, H. (2019) Conformational Change of Amyloid- β 40 in Association with Binding to GM1-Glycan Cluster. *Sci. Rep.* 9, 6853.
- (85) Vivekanandan, S., Brender, J. R., Lee, S. Y., and Ramamoorthy, A. (2011) A partially folded structure of amyloid-beta (1–40) in an aqueous environment. *Biochem. Biophys. Res. Commun.* 411, 312–316.
- (86) Ledeen, R. (1978) Ganglioside structures and distribution: are they localized at the nerve ending? *J. Supramol. Struct.* 8, 1–17.
- (87) Amaro, M., Šachl, R., Aydogan, G., Mikhalyov, I. I., Vácha, R., and Hof, M. (2016) GM1 Ganglioside Inhibits β -Amyloid Oligomerization Induced by Sphingomyelin. *Angew. Chem., Int. Ed.* 55, 9411–9415.
- (88) Ariga, T., McDonald, M. P., and Robert, K. Y. (2008) Thematic Review Series: Spingolipids. Role of ganglioside metabolism in the pathogenesis of Alzheimer's disease—a review. *J. Lipid Res.* 49, 1157–1175.
- (89) Tomaselli, S., Esposito, V., Vangone, P., van Nuland, N. A., Bonvin, A. M., Guerrini, R., Tancredi, T., Temussi, P. A., and Picone, D. (2006) The α -to- β conformational transition of Alzheimer's A β -(1–42) peptide in aqueous media is reversible: A step by step conformational analysis suggests the location of β conformation seeding. *ChemBioChem* 7, 257–267.
- (90) Jorgensen, W. L., Chandrasekhar, J., Madura, J. D., Impey, R. W., and Klein, M. L. (1983) Comparison of simple potential functions for simulating liquid water. *J. Chem. Phys.* 79, 926–935.
- (91) Kaminski, G. A., Friesner, R. A., Tirado-Rives, J., and Jorgensen, W. L. (2001) Evaluation and reparametrization of the OPLS-AA force field for proteins via comparison with accurate quantum chemical calculations on peptides. *J. Phys. Chem. B* 105, 6474–6487.
- (92) Kulig, W., Pasenkiewicz-Gierula, M., and Róg, T. (2015) Topologies, structures and parameter files for lipid simulations in GROMACS with the OPLS-aa force field: DPPC, POPC, DOPC, PEPC, and cholesterol. *Data Brief* 5, 333–336.
- (93) Maciejewski, A., Pasenkiewicz-Gierula, M., Cramariuc, O., Vattulainen, I., and Rog, T. (2014) Refined OPLS all-atom force field for saturated phosphatidylcholine bilayers at full hydration. *J. Phys. Chem. B* 118, 4571–4581.
- (94) Hess, B., Kutzner, C., van der Spoel, D., and Lindahl, E. (2008) GROMACS 4: algorithms for highly efficient, load-balanced, and scalable molecular simulation. *J. Chem. Theory Comput.* 4, 435–447.
- (95) Zhang, J. (2015) The Hybrid Idea of (Energy Minimization) Optimization Methods Applied to Study Prion Protein Structures Focusing on the beta2-alpha2 Loop. *Biochem. Pharmacol. (Los Angeles, CA, U. S.)* 4, 1000175.
- (96) Müller, K., and Brown, L. D. (1979) Location of saddle points and minimum energy paths by a constrained simplex optimization procedure. *Theor. Chim. Acta* 53, 75–93.
- (97) Bussi, G., Donadio, D., and Parrinello, M. (2007) Canonical sampling through velocity rescaling. *J. Chem. Phys.* 126, 014101.
- (98) Parrinello, M., and Rahman, A. (1980) Crystal structure and pair potentials: A molecular-dynamics study. *Phys. Rev. Lett.* 45, 1196.
- (99) Parrinello, M., and Rahman, A. (1981) Polymorphic transitions in single crystals: A new molecular dynamics method. *J. Appl. Phys. (Melville, NY, U. S.)* 52, 7182–7190.
- (100) Parrinello, M., and Rahman, A. (1982) Strain fluctuations and elastic constants. *J. Chem. Phys.* 76, 2662–2666.
- (101) Nosé, S. (1984) A unified formulation of the constant temperature molecular dynamics methods. *J. Chem. Phys.* 81, 511–519.
- (102) Nosé, S. (1986) An extension of the canonical ensemble molecular dynamics method. *Mol. Phys.* 57, 187–191.
- (103) NOSE, S. U. I. (2002) A molecular dynamics method for simulations in the canonical ensemble. *Mol. Phys.* 100, 191–198.
- (104) Hoover, W. G. (1985) Canonical dynamics: Equilibrium phase-space distributions. *Phys. Rev. A: At., Mol., Opt. Phys.* 31, 1695.
- (105) Darden, T., York, D., and Pedersen, L. (1993) Particle mesh Ewald: An N-log(N) method for Ewald sums in large systems. *J. Chem. Phys.* 98, 10089–10092.
- (106) Essmann, U., Perera, L., Berkowitz, M. L., Darden, T., Lee, H., and Pedersen, L. G. (1995) A smooth particle mesh Ewald method. *J. Chem. Phys.* 103, 8577–8593.

- (107) Hess, B., Bekker, H., Berendsen, H. J., and Fraaije, J. G. (1997) LINCS: a linear constraint solver for molecular simulations. *J. Comput. Chem.* *18*, 1463–1472.
- (108) Bussi, G. (2014) Hamiltonian replica exchange in GROMACS: a flexible implementation. *Mol. Phys.* *112*, 379–384.
- (109) Tribello, G. A., Bonomi, M., Branduardi, D., Camilloni, C., and Bussi, G. (2014) PLUMED 2: New feathers for an old bird. *Comput. Phys. Commun.* *185*, 604–613.
- (110) Abraham, M. J., Lindahl, E., Hess, B., and van der Spoel, D., and the GROMACS development team (2018) *GROMACS User Manual*, version 2018.2. www.gromacs.org (accessed Jan 21, 2020).
- (111) Abraham, M. J., Murtola, T., Schulz, R., Páll, S., Smith, J. C., Hess, B., and Lindahl, E. (2015) GROMACS: High performance molecular simulations through multi-level parallelism from laptops to supercomputers. *SoftwareX* *1*, 19–25.
- (112) Páll, S., Abraham, M. J., Kutzner, C., Hess, B., and Lindahl, E. (2015) *Solving Software Challenges for Exascale. International Conference on Exascale Applications and Software, Stockholm, Sweden, April 2–3, 2014* (Laure, S. M., Ed.) pp 3–27, Springer, Cham.
- (113) Pronk, S., Páll, S., Schulz, R., Larsson, P., Bjelkmar, P., Apostolov, R., Shirts, M. R., Smith, J. C., Kasson, P. M., van der Spoel, D., and Hess, B. (2013) GROMACS 4.5: a high-throughput and highly parallel open source molecular simulation toolkit. *Bioinformatics* *29*, 845–854.
- (114) Kabsch, W., and Sander, C. (1983) Dictionary of protein secondary structure: pattern recognition of hydrogen-bonded and geometrical features. *Biopolymers* *22*, 2577–2637.
- (115) Daura, X., Gademann, K., Jaun, B., Seebach, D., van Gunsteren, W. F., and Mark, A. E. (1999) Peptide folding: when simulation meets experiment. *Angew. Chem., Int. Ed.* *38*, 236–240.
- (116) Humphrey, W., Dalke, A., and Schulten, K. (1996) VMD: visual molecular dynamics. *J. Mol. Graphics* *14*, 33–38.

■ NOTE ADDED AFTER ASAP PUBLICATION

Due to a production error, this paper was published on the Web on January 30, 2020, with the wrong Supporting Information file. The corrected version was reposted on February 3, 2020.